JOURNAL OF GUIDANCE, CONTROL, AND DYNAMICS
Vol. 29, No. 6, November–December 2006

Attitude Determination Using a Single-Star Sensor and a Star-Density Table

Jinchun Wang* and Joohwan Chun†
Korea Advanced Institute of Science and Technology, Daejeon 305-701, South Korea

DOI: 10.2514/1.17249

An alternative approach to attitude determination using a star sensor is presented. Whereas conventional star trackers require star vector observations through an identification of star constellations and a tracking of the identified stars, the proposed method takes multiple vector observations of virtual lines of sight instead of stars. A virtual line of sight is the pointing direction of a small portion of a star sensor's field of view and the vector to this line of sight is measured by searching celestial positions having the same theoretical star densities with the measurements, defined as the number of detected stars in the field of view. The suggested approach is based on the fact that the distribution of stars in the sky is not homogeneous. A stepwise search method to determine the pointing directions of multiple lines of sight that give the vector observation sequences is proposed, and a simple least-squares solution is applied for the attitude determination using these vector sequences. The proposed method allows not only a stabilized spacecraft but also a rotational one to take measurements; in the latter case the vector observations of stars are usually difficult owing to the sensor's motion.

I. Introduction

ATTITUDE determination specifies the orientation of the body-fixed (BF) coordinate frame with respect to a given reference coordinate system. The attitude determination of a spacecraft or satellite is usually executed using a combination of sensors and mathematical models. Several different algorithms that represent the attitude in the form of a direct cosine matrix (DCM) [1], a quaternion [2], Euler angles [3], Rodrigues parameters [4], or modified Rodrigues parameters [5] have been developed to determine the attitude. Methods have been devised to solve the attitude determination problem using the vector measurements of the body and the reference frame through a direct method or a filtering method. The Triad algorithm only uses two reference vectors and is one of the simplest algorithms [6]. Wahba proposed a least square estimate method [7]. In addition to an analytical solution to the Wahba problem [8], various numerical solutions have been proposed [9–16]. These methods require at least two vectors to estimate the attitude. Many other algorithms need estimates of the body's angular rates, which can be obtained by gyro measurements because they use the dynamics of spacecraft to estimate the attitude [17].

A sun sensor measures a sun vector, a magnetometer measures a magnetic field vector, and a star sensor measures a star vector to obtain the vector measurements. We can obtain vector measurements by using a single sensor or a fusion of multiple sensors [18]. With the recent advancement in imaging sensor technologies, the star sensor, mounted on a spacecraft, is one of the most popular [19,20]. Although a star tracker, which uses a star sensor and an onboard star catalog to estimate the attitude of a spacecraft, gives a very accurate attitude estimate, the star tracker needs high computational power to identify star constellations [21]. In addition, in the case of a spinning spacecraft, accurate star vector measurements are not easy because a star makes a streak in the image plane. When a spacecraft slews with an angular rate, the vector observations require high update rates resulting low signal-to-noise ratio (SNR). This situation can be relaxed by compensating the spacecraft's rotation to make a star sensor fixed in inertial space. However, this technique, called time-delayed integration (TDI), needs information about precise angular rates and raises the cost of the mission for a precision gauge. Moreover, a gyroless single sensor attitude determination method is required to fulfill a growing demand for small and inexpensive up-to-date satellites.

To overcome the difficulties of star constellation identification with a star pattern matching and those arisen from the streaks of stars in the star vector observations, we propose a method to get multiple vector observations for attitude determination, which uses the number of detected stars in the field of view (FOV) of a star sensor as a measurement. We have previously presented a similar approach to obtain vector observations with this selection of a measurement [22]. The previous approach needs two star sensors with a gyro to determine the attitude and requires high computational power to evaluate the measurements with a bootstrap filter. In this paper, however, we have designed a new method, which determines the attitude using a single star sensor without any auxiliary sensors and derives a more sophisticated measurement model than the previous one. We determine the pointing direction of the star sensor boresight on the celestial sphere. The general idea for that purpose is as follows. The FOV of the star sensor is divided into several small portions called sub-FOV. Then, on one hand, one counts the number of stars above a given magnitude that are detected in each sub-FOV, and on the other hand, one predicts the number of stars that should be detected for a given pointing direction of the star sensor from a star catalog. The optimal pointing direction is obtained by applying various best-fit techniques. As the measurements are processed in a single frame, the proposed method is a single-frame determination method that does not require gyro data, and can be applied to a spinning body because the proposed method counts only the number of stars or star streaks.

The proposed method also has limitations compared to conventional star trackers. It usually requires a large FOV resulting in sun or Earth blockage. Under these blockage situations, it will not be able to operate because the star sensor must count all stars in the FOV. This problem can be mitigated by using more than one star sensor pointing in different directions. The proposed algorithm will fail to operate if a spacecraft rotates too fast to detect star streaks due to low SNR. However, not all applications need vector observations under this high angular rate.

This paper comprises the following: In Sec. II, brief reviews of attitude representations and an attitude determination method are

Received 22 May 2005; revision received 19 March 2006; accepted for publication 20 March 2006.

*Ph.D. Candidate, Division of Electrical Engineering, Department of Electrical Engineering & Computer Science, 373-1 Guseong-dong, Yuseong-gu; jcwang@sclab.kaist.ac.kr

†Professor, Division of Electrical Engineering, Department of Electrical Engineering & Computer Science, 373-1 Guseong-dong, Yuseong-gu; chun@sclab.kaist.ac.kr

given. In Sec. III, a mathematical measurement model is derived; this model is used for the creation of star-density maps. The attitude determination method via two steps of estimation is developed in Sec. IV. In Sec. V, several examples from simulation studies are presented. Finally, our concluding remarks are described in Sec. VI.

II. Problem Statement

In this section, we briefly review some preliminaries such as attitude representations and an attitude determination method. We then describe our approaches to the problem attacked in this paper.

A. Attitude Representation

Attitude means the orientation of a BF coordinate frame $\mathcal{V}$ with respect to the reference coordinate system $\mathcal{U}$. Because all the measurable star vectors necessary for attitude determination are specified with an Earth-centered-inertial (ECI) coordinate in the star catalog, we selected the ECI coordinate system as the reference frame. Various parameters can be used to represent the attitude of a body frame [23]. In our work, the attitude is parameterized by the 4×1 quaternion $\boldsymbol{q}$ and the 3×3 DCM A. The quaternion is a unit vector in $\mathbb{R}^4$ and composed of a vector and scalar part as

$$\boldsymbol{q} = [q_1, q_2, q_3, q_4]^T = [\boldsymbol{v}, q_4]^T \tag{1}$$

where the superscript T represents the transpose. The attitude representation with a quaternion is related to the rotation axis and the rotation angle, which is necessary to align the body frame to the reference frame as

$$\boldsymbol{v} = \boldsymbol{n} \sin(\theta/2), \qquad q_4 = \cos(\theta/2) \tag{2}$$

where $\boldsymbol{n}$ is a unit vector corresponding to the axis of rotation and θ is the angle of rotation.

A unit vector $\boldsymbol{r}$ in $\mathcal{U}$ is transformed to the unit vector $\boldsymbol{b}$ in $\mathcal{V}$ via the DCM A:

$$\boldsymbol{b} = A\boldsymbol{r} \tag{3}$$

The relationship between the DCM and the equivalent quaternion can be described as follows:

$$A(\boldsymbol{q}) = \left(q_4^2 - \boldsymbol{v}^T\boldsymbol{v}\right)I_{3\times3} + 2\boldsymbol{v}\boldsymbol{v}^T - 2q_4[\boldsymbol{v}\times] \tag{4}$$

Here, $I_{3\times3}$ is the 3×3 identity matrix and the cross-product matrix $[\boldsymbol{v}\times]$ is defined as

$$[\boldsymbol{v}\times] \triangleq \begin{bmatrix} 0 & -q_3 & q_2 \\ q_3 & 0 & -q_1 \\ -q_2 & q_1 & 0 \end{bmatrix} \tag{5}$$

B. Attitude Determination

From Eq. (3), the attitude matrix can be determined by a deterministic method that uses vector measurements. However, because this measurement usually has a measurement error, we should apply some numerical methods to estimate the DCM. In this case, the measurement model is

$$\boldsymbol{b} = A\boldsymbol{r} + \delta\boldsymbol{b} \tag{6}$$

where $\delta\boldsymbol{b}$ is the measurement error. The attitude estimation now can be formulated as a least-squares problem from multiple vector observations. That is, if we observe a set of vectors, $\boldsymbol{b}_i (i = 1, 2, \cdots, N)$ where N is the number of vector observations, in the BF frame, and we know the corresponding set of vectors, $\boldsymbol{r}_i$, in the ECI coordinate, the DCM can be estimated by finding the DCM A, which minimizes

$$\sum_{i=1}^{N} \|\boldsymbol{b}_i - A\boldsymbol{r}_i\|^2 \tag{7}$$

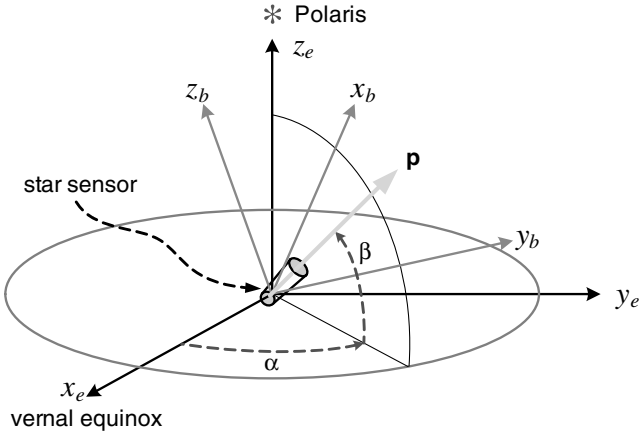

Fig. 1 Coordinate systems. The ECI coordinate system (x_e, y_e, z_e) and the body-fixed frame (x_b, y_b, z_b).

where $\|\cdot\|^2$ denotes a vector L^2-norm, subject to the constraints $A^TA = I_{3\times3}$ and $\det(A) = 1$. This attitude determination problem is well known as the Wahba problem [7].

C. Solution Approach

For attitude determination, we first measure physical vectors in the BF frame and find the corresponding vectors in the ECI coordinate system. Most previous methods using star sensors observe the star vector, which is the unit directional vector of LOS to the star, and obtain the corresponding reference vector from the star catalog by identifying star constellations using point-matching algorithms. A directional vector is specified in the ECI coordinates with two angles called the right ascension (RA) α and the declination (Dec) β by projecting the vector onto the celestial sphere, which is a unit hypersphere $\mathbb{S}^3$, as shown in Fig. 1. The unit vector $\boldsymbol{r} = [r_1, r_2, r_3]^T$'s Cartesian coordinate can be converted to the celestial position $\boldsymbol{x} = [\alpha, \beta]^T$ as

$$\boldsymbol{x} = f_{\text{cs}}(\boldsymbol{r}) = \begin{bmatrix} \arctan(r_2/r_1) \\ \sin^{-1}(r_3) \end{bmatrix} \tag{8}$$

where $f_{\text{cs}}(\cdot)$ transforms a Cartesian coordinate into the spherical (celestial) coordinate and the degree unit is used.

In our method, instead of observing a specific star to obtain the directional vector, we set up a sequence of directional vectors of sub-FOVs around the optical axis of the star sensor in the BF frame and find the corresponding vectors in the ECI coordinate system by comparing the number of detected stars from each sub-FOV and the references obtained from a mathematical model.

III. Mathematical Model

To avoid difficulties arising from the star vector measurement, we select the star density, i.e., the number of stars, in the FOV of star sensor as a new measurement. A reference star-density map that covers the whole celestial sphere can be formulated from a star catalog. We derived a mathematical model to create the density map with a probabilistic detection model.

A. Measurement Model

The star catalog used for attitude determination contains star positions given as RA and Dec at some epoch. The star positions reported in the Smithsonian Astrophysical Observatory (SAO) or AGK-3 star catalogs are accurate to approximately 1 arc-sec.

To obtain the statistical response of a star sensor for the number of stars detected inside its FOV from a star catalog, some assumptions as follows are required: First, all the detected stars by the star sensor having a detection threshold are listed in the star catalog. This assumption is not always reasonable when we use an onboard star

catalog, which usually omits double stars and variable stars. However, because the star catalog including all stars brighter than the detection threshold is available and will be used on the ground in our algorithm, this assumption is a plausible one. Second, we have well-defined instrumental magnitudes for all the stars. That is, the mean and the standard deviations of the magnitude are given for each star. Because the standard deviation of magnitude of a star catalog is mainly affected by the sensor's optical characteristics, it is assumed that all stars have an identical standard deviation and Wertz [24] certified this fact. Third, the star sensor has an exact detection threshold represented in the magnitude. Because the spin of a spacecraft usually results in the degradation of SNR and so the detection threshold values varies according to the angular rate, this third assumption is equitable only for a certain range of angular rate with which a sufficient number of stars are detected. Of course, if the angular rate goes over a certain threshold, the detection threshold will go down that no stars are detected. Fourth, the resolution of the star sensor is high enough to separate adjacent stars. Finally, the FOV of the star sensor has a circular shape so that the rotation of the body does not affect the measurement value.

Now, we derive the statistical response of the star sensor to count the number of stars in the FOV. Let N_p be the total number of stars in the FOV when the direction of the optical axis of the star sensor points to the location $\boldsymbol{x}$ and let m_{th} be the magnitude threshold of the star sensor for the detection of stars. The magnitude of the i_{th} star is normally distributed, $\mathcal{N}(m_i, \sigma^2)$, from the second assumption. Therefore, the detection probability of the i_{th} star is given by

$$p_i = P[m_i \le m_{\text{th}}] = \int_{-\infty}^{m_{\text{th}}} \frac{1}{\sqrt{2\pi}\sigma} \exp\left(-\frac{(x-m_i)^2}{2\sigma^2}\right) \mathrm{d}x \quad (9)$$

Here, the inequality sign and the range of integral was chosen that way because the brighter the star is, the lower magnitude it has. Let $s_i \in \{0, 1\}$ be a random variate for the i_{th} star of N_p where $s_i = 1$ means that the i_{th} star is detected by the star sensor. By using Eq. (9), the mean μ_i and variance σ_i^2 of s_i are given by

$$\mu_i = p_i \quad (10)$$

$$\sigma_i^2 = p_i(1 - p_i) \quad (11)$$

Let $(s_1, s_2, \ldots, s_{N_p})$ be a set of N_p independent random variates, and each s_i has a binomial distribution with a mean and a finite variance given in Eqs. (10) and (11). Let n_p be defined as $n_p = s_1 + s_2 + \cdots + s_{N_p}$. If N_p is a sufficiently large number to apply the central limit theorem, then the random variate n_p is approximately normally distributed with [25]

$$\mu_{n_p} = \sum_{i=1}^{N_p} p_i \quad (12)$$

$$\sigma_{n_p}^2 = \sum_{i=1}^{N_p} p_i(1 - p_i) \quad (13)$$

Consequently, when N_p stars with different means and the same variance exist inside the FOV for a given orientation of the star sensor, the number of stars detected by the star sensor has a normal distribution.

B. Star-Density Map

Figure 2 shows the distributions of stars brighter than 6.0 magnitude extracted from the SAO star catalog, which contains 258,996 stars. Because the density of the cloud varies according to the RA and Dec, as shown in Fig. 2, the star-density map also depends on the location, the FOV size, and the magnitude threshold of the star sensor.

The derived mathematical model allows one to make star-density mean and variance maps, which are two-dimensional (2-D) maps that

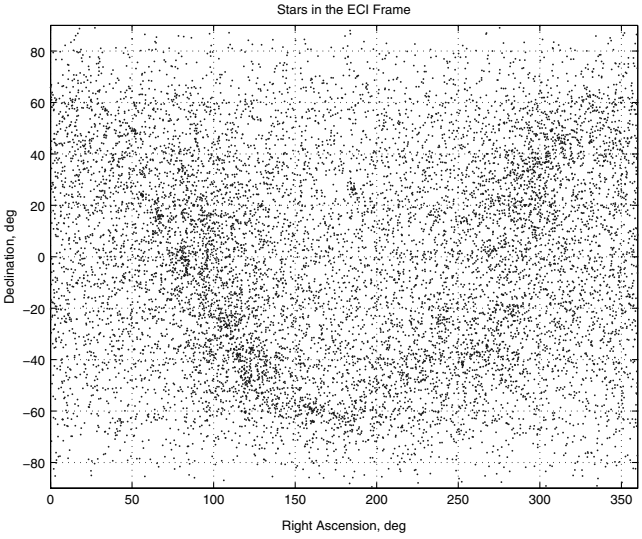

Fig. 2 Distribution of stars brighter than 6.0 magnitude from the SAO star catalog.

have linear grids with respect to RA and Dec; the value at the grid point is given by Eqs. (12) and (13), respectively. From the geometry in Fig. 1, the vector of the sensor's optical axis $\boldsymbol{p}$, represented by the Cartesian coordinate, is mapped into RA and Dec, $\boldsymbol{x} = [\alpha, \beta]^T$, in the celestial coordinate system. Therefore, for given $\boldsymbol{p}$, the reference star-density map is subject to the celestial position $\boldsymbol{x}$, the star sensor's FOV ϕ, and the threshold of the magnitude, m_{th}, of the star sensor: $h(\boldsymbol{x}, \phi, m_{\text{th}})$. Suppose that whole stars contained in SAO star catalog are considered, and the star sensor has $m_{\text{th}} = 6.0$ with $\phi = 15$ deg; the star-density mean map, $h_\mu(\boldsymbol{x})$, and the variance map, $h_\sigma(\boldsymbol{x})$, are shown in Fig. 3. Here, m_{th} and ϕ are omitted because there is no ambiguity. The grid size of each star-density map is 1 deg, as shown in Fig. 3. When $\boldsymbol{x}$ is not located on the grid point, the map value is computed by the bilinear interpolation as

$$\begin{aligned}\mathcal{I}[h(\alpha_0, \beta_0)] &= h(\alpha_1, \beta_1) + h(\alpha_2, \beta_1)(\alpha_0 - \alpha_1) \\ &\quad + h(\alpha_1, \beta_2)(\beta_0 - \beta_1) + \{h(\alpha_1, \beta_1) + h(\alpha_2, \beta_2) \\ &\quad - h(\alpha_1, \beta_2) - h(\alpha_2, \beta_1)\}(\alpha_0 - \alpha_1)(\beta_0 - \beta_1) \end{aligned} \quad (14)$$

where $\mathcal{I}[h(\alpha_0, \beta_0)]$ is the interpolated value at the position $\boldsymbol{x} = [\alpha_0, \beta_0]^T$ and $[\alpha_i, \beta_i]^T$ for $i = 1, 2$ is a grid point.

Finally, the measured number of stars detected by the star sensor is modeled as

$$z_k = \lceil \mathcal{I}[h_\mu(\boldsymbol{x})] + \eta(\boldsymbol{x}) \rceil \quad (15)$$

where $\lceil \cdot \rceil$ is a ceiling operator, which denotes the quantization error, and $\mathcal{I}[\cdot]$ is the bilinear operator. Here, η is the digitization error caused by a bilinear interpolation. The digitization error has a uniform distribution whose mean and variance are dependent on the state vector of the sample and the four grid values of the star-density map surrounding the sample.

IV. Attitude Determination Method

The preferred directional vector, which we can easily select in the BF frame, is the directional vector of the optical axis of the star sensor. Although we can estimate the orientation of this single observation, it is necessary to get more directional vector observations to estimate an unambiguous attitude because of the ambiguity of rotation. For this reason, we set up a sequence of directional vectors with the optical axes of sub-FOVs. The sub-FOV is defined as a virtual FOV covering a small portion in the physical FOV, called the main-FOV in this paper, of the star sensor. As shown in Fig. 4, we establish the sub-FOVs as inscribed circles to the

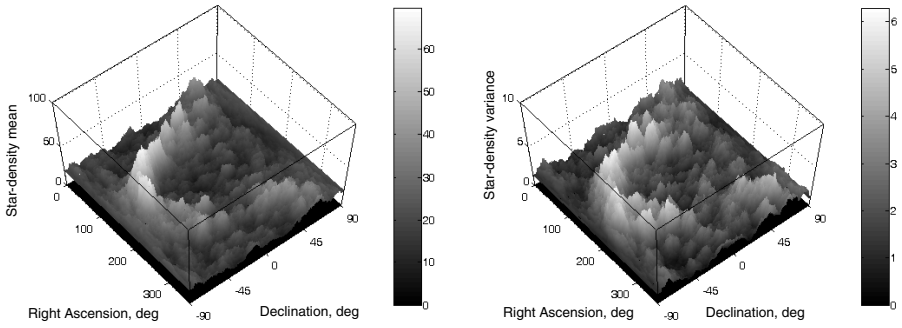

a) b)

Fig. 3 a) Star-density mean map and b) star-density variance map; $m_{\text{th}} = 6.0$ and $\phi = 15$ deg.

main-FOV. Note that the sub-FOV is a conceptional FOV, which requires no physical sensor. The angle ψ between the directional unit vector of the main-FOV, $\boldsymbol{p}^m$, and that of sub-FOV, $\boldsymbol{p}_i^s$, satisfies the following relationship:

$$\psi = \cos^{-1}\left(\frac{(\boldsymbol{p}^m)^T \boldsymbol{p}_i^s}{\|\boldsymbol{p}^m\|\|\boldsymbol{p}_i^s\|}\right) = \frac{\phi_m}{2} - \frac{\phi_s}{2} \tag{16}$$

where $\|\cdot\|$ is a vector L^2-norm, ϕ_m is the main-FOV angular diameter, and ϕ_s is the sub-FOV angular diameter. For notational simplification, we set $\boldsymbol{p}^m = [1, 0, 0]^T$. This setting means that the star sensor is oriented along the x-axis of the BF frame. The directional vector of the optical axis of ith sub-FOV, $\boldsymbol{p}_i^s$, can then be calculated as

$$\boldsymbol{p}_i^s = \begin{bmatrix} \cos\psi \\ \sin\psi\cos\gamma_i \\ \sin\psi\sin\gamma_i \end{bmatrix} \tag{17}$$

where $\gamma_i = 360(i-1)/N_s$ deg for $i = 1, \cdots, N_s$ when N_s is the number of virtual sub-FOVs.

A. Coarse Attitude Estimation Using Sequence Matching

Now, we can estimate the attitude by finding the view positions or ECI coordinates of the sequence of virtual directional vectors and solving Eq. (7) using these vectors. The search for the ECI coordinates of the optical axis can be performed through sequence matching between the sub-FOV measurements and the star-density map.

1. *Prefiltering*

Basically, we can search full areas of the star-density map to find the celestial position of the optical axis of the main-FOV. When a search is performed only on the grid points of the map, however, a total of 64, 800(=360 × 180) matching function evaluations should be performed. This full-search strategy is cumbersome and time-consuming work. To overcome this problem, we select candidate points by using a prefiltering approach. The basic idea is to select grid points having the measurements of the given FOV before sequence matching. Because the number of grid points having the same number of stars may still be too large under the main-FOV measurement constraint alone, we can force an additional FOV measurement condition by changing the angle of the FOV, as shown in Fig. 4. To accomplish the aforementioned procedure, we exclude grid points that do not satisfy the following conditions:

$$\begin{cases} h_\mu(\boldsymbol{x}, \phi_m) - \kappa h_\sigma(\boldsymbol{x}, \phi_m) \le z_{\phi_m}(\boldsymbol{p}^m) \le h_\mu(\boldsymbol{x}, \phi_m) + \kappa h_\sigma(\boldsymbol{x}, \phi_m) \\ h_\mu(\boldsymbol{x}, \phi_n) - \kappa h_\sigma(\boldsymbol{x}, \phi_n) \le z_{\phi_n}(\boldsymbol{p}^m) \le h_\mu(\boldsymbol{x}, \phi_n) + \kappa h_\sigma(\boldsymbol{x}, \phi_n) \end{cases} \tag{18}$$

where $\phi_n (< \phi_m)$ is a prefiltering FOV angle, $z_\phi(\boldsymbol{p})$ means the measurement of FOV ϕ with a unit vector $\boldsymbol{p}$ of optical axis, and κ is a constant to control the number of candidate points.

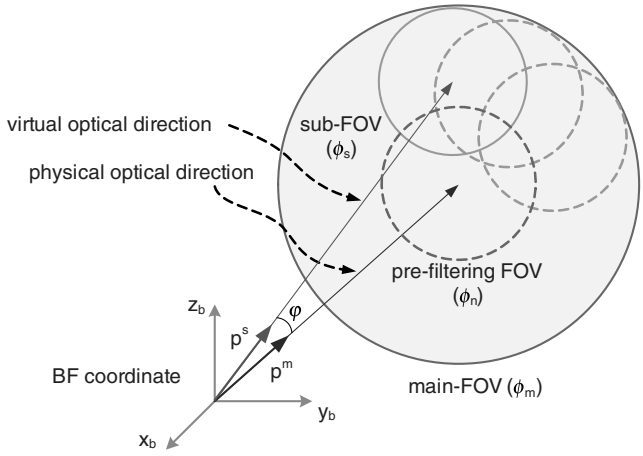

Fig. 4 Sub-FOV concept.

2. *Sequence Matching*

We should determine the right position of $\boldsymbol{p}^m$ among the candidate positions obtained by using prefiltering. This process can be accomplished by selecting the candidate position that gives the maximum sequence-matching value with the observed measurement sequence. Let the measurements sequence be denoted by $\boldsymbol{z} = \{z_{\phi_s}(\boldsymbol{p}_1^s), \cdots, z_{\phi_s}(\boldsymbol{p}_{N_s}^s)\}$ and sample the star-density map around a candidate point to make a template sequence $\boldsymbol{h}_j = \{h_\mu(\boldsymbol{x}_1^j, \phi_s), \cdots, h_\mu(\boldsymbol{x}_{N_s}^j, \phi_s)\}$ for $j = 1, 2, \cdots, N_c$, where N_c is the number of candidate points resulting from prefiltering and $\boldsymbol{x}_i^j$ is the celestial position that corresponds to the directional vector of the virtual optical axis $\boldsymbol{p}_i^s$ when the physical optical axis is mapped onto the candidate point j in the celestial coordinate. Note that although the origins of the virtual sub-FOV describe a circle in the BF frame, $\boldsymbol{x}_i^j$ does not shape a circle in the star-density map because the spherical coordinate is mapped onto the 2-D Cartesian coordinate. The determination of $\boldsymbol{x}_i^j$ at a candidate position $\boldsymbol{x}_c$, or $\boldsymbol{p}_c$ in the Cartesian coordinate, is accomplished by first posing a directional vector $\boldsymbol{p}_t$, which forms an angle of ψ with $\boldsymbol{p}_c$ with same Dec β, and, next, rotating $\boldsymbol{p}_t$ with the rotation axis $\boldsymbol{p}_c$ and rotation angle $\theta_k = 360(k-1)/N_s$ for $k = 1, \cdots, N_s$. These processes can be performed using the quaternion and Eq. (4) as

$$\boldsymbol{y}_k^j = A(\boldsymbol{q}_k) \cdot \boldsymbol{p}_t \tag{19}$$

where

$$\boldsymbol{q}_k = \begin{bmatrix} \sqrt{1 - \cos^2(\theta_k/2)} \cdot \boldsymbol{p}_c \\ \cos(\theta_k/2) \end{bmatrix}, \qquad k = 1, 2, \cdots, N_s \tag{20}$$

Here, $\boldsymbol{y}_k^j$ is the vector of the Cartesian coordinates corresponding to $\boldsymbol{x}_k^j$.

Given the sets of N_s vectors $\boldsymbol{z}$ and $\boldsymbol{h}_j$, we find the proper $\boldsymbol{h}_j$, which brings the best match with $\boldsymbol{z}$. A correlation between the measurement

sequence and a reference sequence provides a matching measurement. However, $\boldsymbol{h}_j$ should be reformulated for all possible rotations because we know only the point corresponding to the rotation axis, not the point corresponding to the rotation angle. Reformulated sequences are the circular shifted versions of $\boldsymbol{h}_j$ and have N_s cases. To avoid computing correlations for $N_s \times N_c$ cases and to obtain the rotation-invariant property, we apply the fast Fourier transform (FFT) to $\boldsymbol{h}_j$ and $\boldsymbol{z}$. The selection of the best match finds j, which maximizes

$$m_c = \max_j \{\text{corr}(|\text{FFT}(\boldsymbol{h}_j)|, |\text{FFT}(\boldsymbol{z})|)\}, \qquad j = 1, 2, \cdots, N_c \tag{21}$$

Here, $\text{corr}(\boldsymbol{m}, \boldsymbol{n})$ means the correlation between the two vectors $\boldsymbol{m}$ and $\boldsymbol{n}$, $\text{FFT}(\cdot)$ is the elementwise FFT, and $|\cdot|$ is the complex norm. Finally, to obtain the rotational factor, we compute the correlations for all circular shifted sequences and choose the maximum as follows:

$$n_s = \max_i \{\text{corr}(\boldsymbol{h}^i_{m_c}, \boldsymbol{z})\} \tag{22}$$

where $\boldsymbol{h}^i_{m_c}$ is the ith circular shifted vector of $\boldsymbol{h}_{m_c}$ for $i = 0, 1, \cdots, N_s - 1$. The preceding calculations of circular correlation and FFT are, in effect, calculating the rotation angle about $\boldsymbol{p}^m$ and give the third axis of attitude, though with a reduced accuracy, which can be increased in proportion to the number of sub-FOVs N_s.

Now, the DCM A can be estimated by solving Eq. (7); this minimization problem is solved in the least-squares sense by the pseudoinverse equation defined by

$$A = RB^T(BB^T)^{-1} \tag{23}$$

where

$$B = \left[\boldsymbol{p}^s_1, \boldsymbol{p}^s_2, \cdots, \boldsymbol{p}^s_{N_s}\right]$$

$$R = \left[\boldsymbol{y}^{m_c}_{n_s+1}, \boldsymbol{y}^{m_c}_{n_s+2}, \cdots, \boldsymbol{y}^{m_c}_{N_s}, \boldsymbol{y}^{m_c}_1, \cdots, \boldsymbol{y}^{m_c}_{n_s}\right]$$

The coarse estimation presented in this section shows the results of the grid resolution, i.e., 1 deg, for the celestial position of the optical axis. It is necessary to subdivide the grid point to obtain a more minute position. This hierarchical approach can be applied iteratively until the designed resolution is achieved.

B. Fine Attitude Estimation Using the Simplex Method

Instead of adopting a hierarchical method that needs a modification of the star-density map to a higher resolution, we can take an optimization approach to estimate the attitude more precisely. We define the following cumulative cost function, which compares the measurements and the reference values of the map:

$$\min_{\boldsymbol{x}^j} J(\boldsymbol{x}^j) = \min_{\boldsymbol{x}^j}\left\{\frac{1}{N_s}\sum_{k=1}^{N_s}\lambda\left\{z_{\phi_s}\left(\left[\boldsymbol{x}^j_k\right]_{n_s}\right)\right\}\left|z_{\phi_s}\left(\boldsymbol{p}^s_k\right)\right.\right.$$
$$\left.\left. - \left\lceil \mathcal{I}\left\{h_\mu\left(\left[\boldsymbol{x}^j_k\right]_{n_s}\right)\right\} + \eta\left(\left[\boldsymbol{x}^j_k\right]_{n_s}\right)\right\rceil\right|\right\} \tag{24}$$

where $[\boldsymbol{x}^j_k]_{n_s}$ is the circular shifted version of $\boldsymbol{x}^j_k$ represented as

$$\left[\boldsymbol{x}^j_k\right]_{n_s} = \begin{cases} \boldsymbol{x}^j_{(k+n_s) \bmod N_s} & \text{for } k \neq N_s - n_s \\ \boldsymbol{x}^j_{N_s} & \text{for } k = N_s - n_s \end{cases}$$

Here, $[\boldsymbol{x}^j_k]_{n_s}$ can be obtained using the procedure of the circular shift correlation of the preceding section. The preceding equation shows that the rotation factor should be founded at each evaluation of the cost function. As shown in Fig. 3, high star-density regions have high variance bringing about a chance of large error. This fact results that a large measurement contributes to the cost function more than a small one regardless of the frequency of unmatched points. To normalize the effect of this inequality, we adopted a normalizing factor $\lambda(z)$.

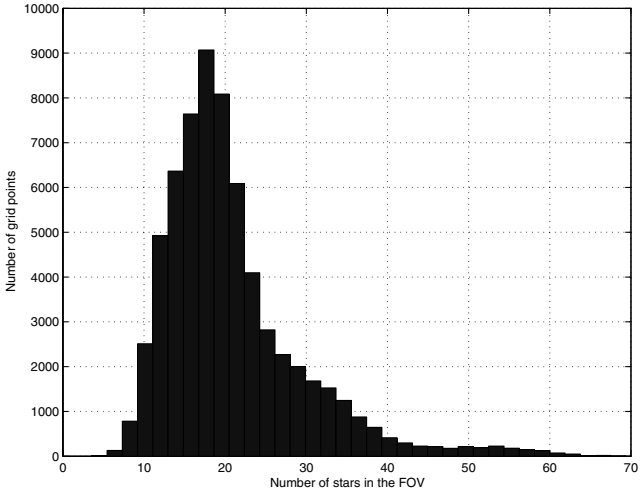

Fig. 5 Measurements distribution for $\phi = 15$ deg.

Figure 5 shows the histogram of the measurement. The x- and y-axes denote the number of stars in the FOV and the number of grid points (bins), respectively. Because the measurement z_k is a nonnegative integer set, the measurement model has a non-Gaussian probability distribution. In Fig. 5, the distribution of measurements is approximately the Erlang, $p(z) \sim \exp[-(z - z_{\text{mean}})/z_{\text{min}}]$, where z_{mean} and z_{min} are the mean and minimum values of the possible measurements. We can estimate the mean value of measurements as about 20 in Fig. 5. As a result, the weighting factor $\lambda(z)$ is determined as $\lambda(z) = \exp(20/z)$ to give a unit weight to the mean value of measurements and a small weight to the large measurements.

One of the suitable optimization algorithms that find the local minimum of Eq. (24) is the downhill simplex method [26]. By setting an initial point $\boldsymbol{x}_0$ as $\boldsymbol{x}^{m_c}$, which is the result of the coarse estimation, we can estimate the more precise position of the optical axis by applying the downhill simplex method. Similar to the coarse estimation, the circular shift correlation and the least-squares solving method are needed after the optimization process to estimate the attitude.

C. Algorithm for a Spinning Case

There are some issues to be carefully considered to use the proposed algorithm with a spinning spacecraft. In the case of a spinning spacecraft, the stars make streaks in the image plane. This results in the degradation of SNR. Moreover, during the integration period, some stars will enter the FOV while some will exit and two star streaks might intersect in the image plane. These will affect to the star count. All these matters can be solved using the TDI technique which compensates for the motion of spacecraft; however, it can only be applied to rotations about an orthogonal spin axis and needs the angular rates. Liebe et al. give very good clues to the solution of the star streaks problems [27]. They proposed a stellar gyroscope, which is a star tracker that can operate at high slew rates and high update rates. In the stellar gyroscope, the spin rate and the spin axis are obtained from the length and the shape of the star streaks and the star streaks are fitted to the spherical circles by projecting the sensing image to the unit sphere. The polarity of the spin also can be determined from the two different images acquired in fast sequence, thus, the start point and the end point of a streak can be discriminated. These techniques can be used to get the number of streaks in the star sensor image.

The degradation of SNR is the inevitable result of spinning, accordingly the detection threshold should be appropriately adjusted. Fortunately, a detection threshold can be calculated for spin rates so that, if we get a spin rate using a stellar gyroscope or a conventional gyroscope, we can determine the detection threshold. Reasonably, the high angular rate over a certain threshold results in a too low detection threshold and the proposed algorithm will not operate. This angular rate threshold depends on the sensor characteristics like the

number of pixels and the sensor sensitivity used in the star sensor. For the case of spinning spacecraft, because the attitude changes during an integration time, we just estimate the attitude at the start time of integration. To count the number of stars in the FOV at the start time, newly entered stars after the start of integration should be excluded from the number of streaks. The number of streaks can be counted by means of a spherical circle fit. Using this spherical circle fitting, two intersected streaks can be discriminated and counted as right because it would be fitted to different spherical circles. The star streaks entered in the FOV during the integration time have the start points on the boundary of the FOV. Among these stars, some are newly entered and the others are on the edge of FOV at start time. Two different images acquired in fast sequence discriminate between the former and the latter because the latter is not present in the previous image. For details on detection threshold adjustment, spherical circle fit, and star streaks, see [27].

D. Storage and Computational Requirements

To compare storage requirements and computational requirements for the proposed method with that of an attitude determination algorithm that must identify individual stars, the star catalog having N_{star} stars and the star-density map of N_g grid points are considered. In the following discussions, although there are many known algorithms that reduce storage requirements or computational requirements, we do not take into account these techniques and roughly calculate the requirements for simplicity. A conventional method which uses three stars to identify constellations require the whole star catalog which includes the right ascension and the declination of each individual star for N_{star} stars. On the other hand, the proposed method needs a star-density mean and variance maps, which have N_g grid points. After all, whereas the conventional method requires $2 \times N_{\text{star}}$ storage, the propose method requires only $4 \times N_g$ storages. Although N_{star} and N_g vary according to the operating situations like the star catalog used, the spacing of the star-density map and the detection threshold m_{th}, N_{star} is usually much larger than N_g. For example, $N_{\text{star}} = 258,996$ and $N_g = 64,800$ are used in our simulation studies in which $m_{\text{th}} = 6$, thus the proposed method uses only 50% storage compared with that of conventional method. It is well known that the conventional method has $\mathcal{O}(N_{\text{star}}^3)$ complexity for whole search to identify star constellations. The proposed method has $\mathcal{O}(N_c N_s \log_2 N_s)$ complexity, which mainly comes from the calculation of FFT in each evaluation of cost function. This is a much lower complexity compared with $\mathcal{O}(N_{\text{star}}^3)$.

V. Simulation Examples

An extensive simulation study was performed to investigate the proposed method through simulated examples. To evaluate the performance of the estimator, a convergence index is defined as [3,4]

$$C \triangleq \|A_{\text{true}} - A_{\text{est}}\|_F^2 \tag{25}$$

where $\|\cdot\|_F$ is the Frobenius norm of a matrix, A_{true} is the true DCM, and A_{est} is the one estimated by the proposed method.

The parameter determination of ϕ_m, ϕ_s, m_{th}, N_s, and κ plays an important role in the performance of the proposed algorithm. The angle of the sub-FOV and the detection threshold are determined in due consideration of the sky coverage, which is defined as the proportion of the celestial points where the suggested method can be applied [28]. Our method will operate even when there are no stars in one of the sub-FOVs, on the condition that there exists a variance between the sub-FOV measurements. However, if we select too small an angle to include stars in the sub-FOV, there will be the increase of possibility of low variance between the measurements because the contour of star-density map has a slow gradient in the most positions. Although it is not a mandatory condition, according to our simulation studies, there is a sufficient variance to operate our algorithm if we choose that all the sub-FOVs have more than one star. We simulated the sky coverage as the percentage of the grid point where more than one star is in the FOV for a successful operation. Figure 6 shows the sky coverage as a function of the FOV for

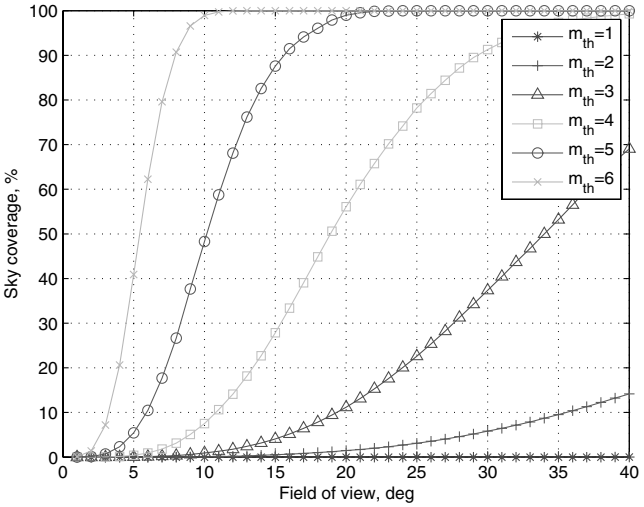

Fig. 6 Sky coverage as a function of the FOV for various magnitudes.

different detection thresholds. The sky coverage should be close to 100% to operate the proposed method at all attitudes, and so we selected the detection threshold as $m_{\text{th}} = 6$ and the sub-FOV as $\phi_s = 15$ deg to give some margins. Because the rest of the parameters are closely related to the celestial position at which they are computed, and a large variance between measurements results in a good match, we should determine the parameters so that the proposed algorithm will operate even at the position of the minimum variance of the measurements. We computed block-variances of star-density mean map by sliding a window of size from 1×1 to 30×30. Here, the block-variance means the variance of star-density mean value in a window and multiple choices of window size are needed due to the uncertainty of the angle of FOV. After averaging these 30 block-variance maps at all the grid points, we selected 50 grid points of minimum block-variance mean map. Figure 7 shows the block-variance mean of 30 block-variance maps and 50 minimum grid points. Now, these 50 grid points are latent positions having the minimum variance of the measurements. To determine the angle of ψ that gives the highest variance in latent minimum variance positions, a variance is computed as a function of ψ at these 50 grid points. Here, the variance is computed with a measurement sequence of 360 sub-FOVs making an angle of ψ with the line of sight of each grid point. The averaged variance of these 50 grid points as a function of ψ is shown in Fig. 8. The angle $\psi = 15$ deg gives the maximum variance in Fig. 8. The main-FOV is therefore $\phi_m = 45$ deg, according to Eq. (16).

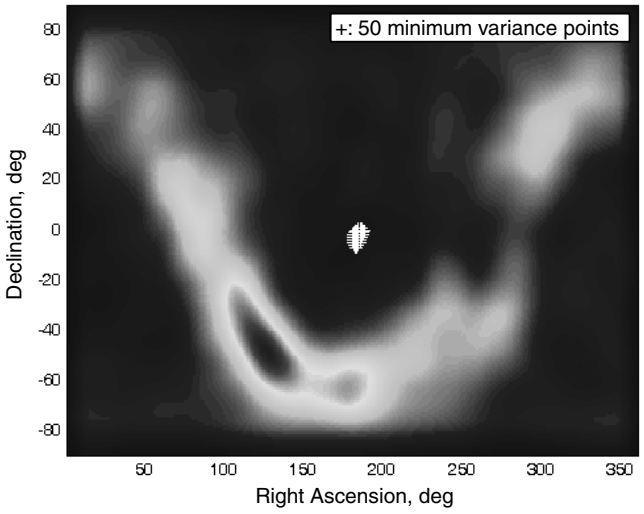

Fig. 7 Variance mean map and 50 minimum variance points.

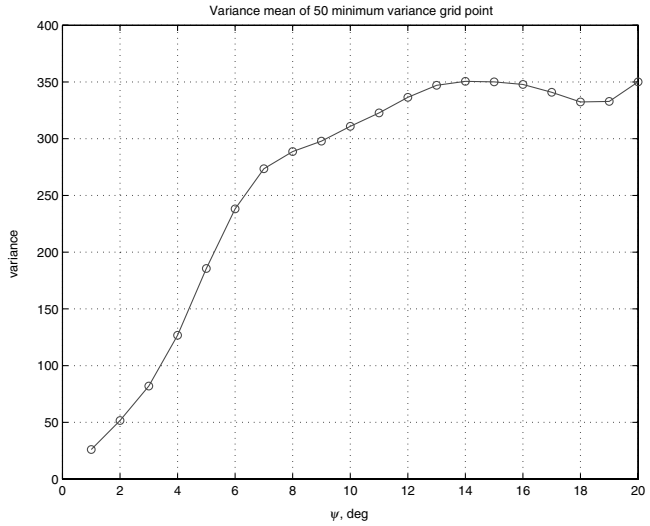

Fig. 8 Variance mean as a function of ψ when $N_s = 360$.

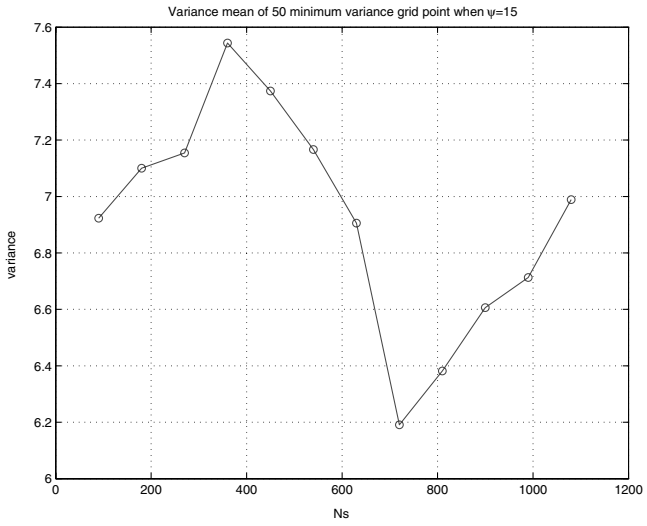

Fig. 9 Variance mean as a function of N_s when $\psi = 15$ deg.

The selection of N_s is related to the accuracy of estimation because it determines the resolution of the rotation factor. However, a large N_s over a certain threshold value not only increases the computational load but also does not increase the resolution due to the limitations of the star-density map resolution. To determine the optimal number of sub-FOVs considering this limitation, the variance mean of 50 minimum variance grid points with $\psi = 15$ deg is plotted as a function of N_s in Fig. 9 and we set $N_s = 360$, which gives an error angle of rotation ranging $-0.5 < e_\theta \leq 0.5$, where e_θ is the rotation error in degrees. Finally, the constant κ of Eq. (18) is chosen as $\kappa = 0.2$; this value always gives sufficient candidates, including the nearest grid point to the true position for all the cases we tried. This value can be modified to obtain a proper candidate number considering the computational capacity of the estimator. Two star-density maps of $m_{\text{th}} = 6.0$ have been created using the measurement model from the SAO star catalog for $\phi_m = 45$ deg and $\phi_n = \phi_s = 15$ deg. The choice of the same angle for ϕ_n and ϕ_s reduces the number of star-density maps necessary for the execution of the algorithm.

The results of a few examples are shown next. In the first example, the attitude is attentively selected so that the optical axis points to the worst position in the sense of the minimum variance to show the robustness of the method. The true attitude is set to $\boldsymbol{q} = [-0.9989, 0.0452, 0.0140, 0.0025]^T$, which maps the main optical axis to the true celestial coordinate $\boldsymbol{x}_m = [185.1834, -1.6179]^T$ deg. Table 1 shows the true attitude and summarizes the simulation environments. Figure 10 presents the true and candidate positions of $\boldsymbol{x}_m$ that satisfy the conditions of Eq. (18). The candidate positions that satisfy the first inequality and the second inequality of Eq. (18) are represented by the point and the asterisk marker, respectively. Although each inequality condition gives much more candidate positions, the total number of candidates satisfying two conditions simultaneously is $N_c = 9$. The coarse estimation with sequence matching gives $\hat{\boldsymbol{x}}_m = [186, -1]^T$. The results obtained with this coarse estimation after finding the virtual directional vectors and applying the least-squares solution are summarized in Table 1. The downhill simplex optimization with the initial value $\boldsymbol{x}_0 = [186, -1]^T$ converges to the more precise estimation as $\hat{\boldsymbol{x}}_m = [185.1808, -1.6196]^T$ in 34 iterations. This fine estimation yields an error of under 100th degree. Figure 11 plots the true and estimated position of $\boldsymbol{x}_m$, and positions of the origins of the virtual sub-FOVs. As shown in Table 1, the convergence index gives an indication of the estimation accuracy of the proposed algorithm. To show that the procedure also matched rotation about the $\boldsymbol{p}_m$, we show the rotation angle θ and the positions of y-axis and z-axis of BF frame in the table.

The parameters used in the preceding example are optimized in the sense of the variance; the main-FOV $\phi_m = 45$ deg may be too wide in comparison with that of conventional star sensors. The next example assumed $\phi_m = 30$ deg to show the feasibility of the algorithm under a plausible main-FOV. The parameters and the results of simulation are summarized in Table 2. In this example, the candidate number after prefiltering is $N_c = 108$, which is larger than that of the first example because the difference between ϕ_m and ϕ_s is

Table 1 True attitude parameters and estimated parameters when $\phi_m = 45$ deg

Parameter	True value	
Position of optical axis, $\boldsymbol{x}_m$	$[185.1834, -1.6179]^T$ deg	
Position of y-axis, $\boldsymbol{x}_y$	$[275.1894, -0.2130]^T$ deg	
Position of z-axis, $\boldsymbol{x}_z$	$[192.6864, 88.3681]^T$ deg	
Rotation angle, θ	179.7135 deg	
DCM, A	$\begin{bmatrix} -0.9955 & -0.0903 & -0.0282 \\ 0.0904 & -0.9959 & -0.0037 \\ -0.0278 & -0.0063 & 0.9996 \end{bmatrix}$	
FOV	$\phi_m = 45$ deg	$\phi_s = \phi_n = 15$ deg
	Coarse estimation	*Fine estimation*
Position of optical axis, $\hat{\boldsymbol{x}}_m$	$[186, -1]^T$ deg	$[185.1808, -1.6196]^T$ deg
Position of y-axis, $\hat{\boldsymbol{x}}_y$	$[276.0198, -1.1315]^T$ deg	$[275.1869, -0.2132]^T$ deg
Position of z-axis, $\hat{\boldsymbol{x}}_z$	$[234.5396, 88.4899]^T$ deg	$[192.6838, 88.3664]^T$ deg
Rotation angle, $\hat{\theta}$	178.8176 deg	179.7138 deg
DCM, $\hat{A}$	$\begin{bmatrix} -0.9944 & -0.1045 & -0.0175 \\ 0.1049 & -0.9943 & -0.0197 \\ -0.0153 & -0.0215 & 0.9997 \end{bmatrix}$	$\begin{bmatrix} -0.9955 & -0.0903 & -0.0283 \\ 0.0904 & -0.9959 & -0.0037 \\ -0.0278 & -0.0063 & 0.9996 \end{bmatrix}$
Convergence index, C	0.0012	5.8380×10^{-9}

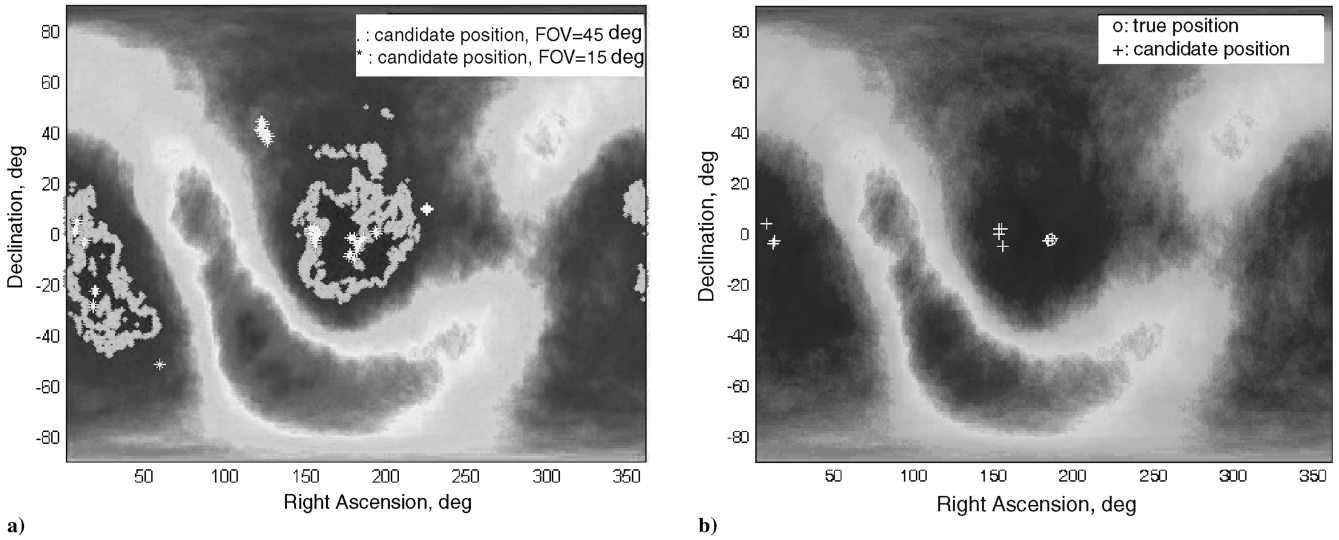

a) b)

Fig. 10 a) Candidate positions when $\phi_m = 45$ deg and $\phi_n = 15$ deg, respectively. b) True position of the main-FOV origin and candidate positions resulted from the prefiltering.

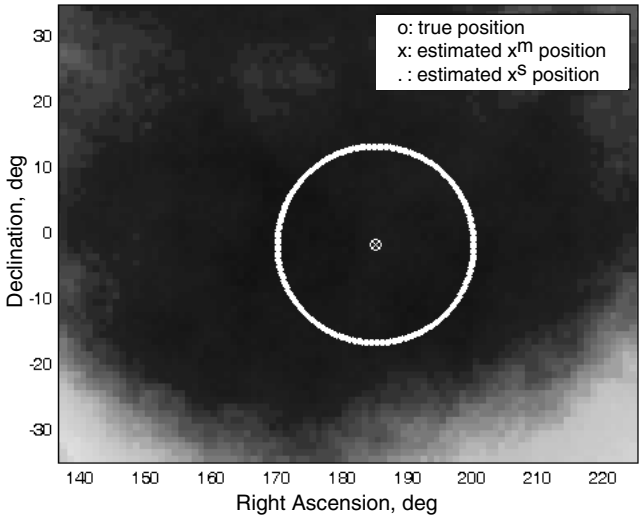

Fig. 11 Result of fine estimation when $\phi_m = 45$ deg.

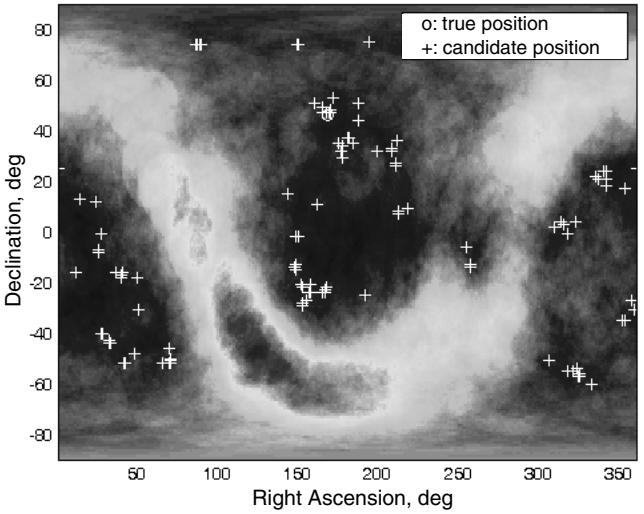

Fig. 12 Result of prefiltering when $\phi_m = 30$ deg.

larger when $\phi_m = 45$ deg compared with the case of $\phi_m = 30$ deg. Figures 12 and 13 show the candidate points after prefiltering and the estimated positions of main-FOV after the fine estimation stage, respectively. The resulted convergence index proves the accommodation of the algorithm in the determination of the LOS of the main-FOV.

Finally, a spinning spacecraft with the angular rate $\omega = [-10, 20, -10]^T$ deg /s is considered. In this case, the detection

Table 2 True attitude parameters and estimated parameters when $\phi_m = 30$ deg

Parameter	True value	
Position of optical axis, $\boldsymbol{x}_m$	$[168.6901, 47.1666]^T$ deg	
Position of y-axis, $\boldsymbol{x}_y$	$[333.4349, 41.8103]^T$ deg	
Position of z-axis, $\boldsymbol{x}_z$	$[70.3462, 7.6623]^T$ deg	
Rotation angle, θ	246.4218 deg	
DCM, A	$\begin{bmatrix} -0.6667 & 0.1333 & 0.7333 \\ 0.6667 & -0.3333 & 0.6667 \\ 0.3333 & 0.9333 & 0.1333 \end{bmatrix}$	
FOV	$\phi_m = 30$ deg	$\phi_s = \phi_n = 15$ deg
	Coarse estimation	*Fine estimation*
Position of optical axis, $\hat{\boldsymbol{x}}_m$	$[168, 48]^T$ deg	$[168.6745, 47.1833]^T$ deg
Position of y-axis, $\hat{\boldsymbol{x}}_y$	$[334.1173, 41.1568]^T$ deg	$[333.6097, 41.8193]^T$ deg
Position of z-axis, $\hat{\boldsymbol{x}}_z$	$[70.2274, 6.9428ey]^T$ deg	$[70.4338, 7.5649]^T$ deg
Rotation angle, $\hat{\theta}$	246.5768 deg	246.5318 deg
DCM, $\hat{A}$	$\begin{bmatrix} -0.6545 & 0.1391 & 0.7431 \\ 0.6774 & -0.3287 & 0.6581 \\ 0.3358 & 0.9341 & 0.1209 \end{bmatrix}$	$\begin{bmatrix} -0.6664 & 0.1335 & 0.7335 \\ 0.6676 & -0.3313 & 0.6668 \\ 0.3320 & 0.9341 & 0.1316 \end{bmatrix}$
Convergence index, C	6.4915×10^{-4}	1.0500×10^{-5}

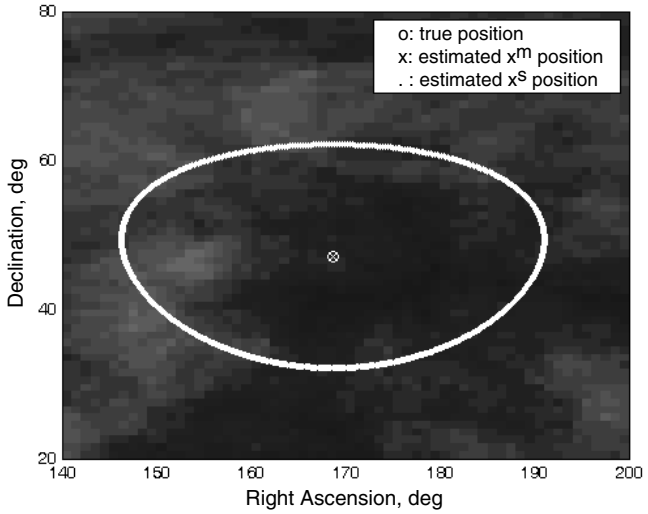

Fig. 13 Result of fine estimation when $\phi_m = 30$ deg.

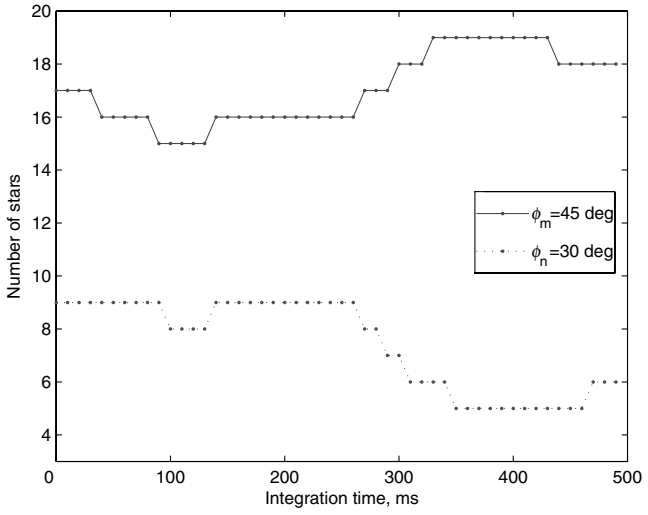

Fig. 14 Changes of the number of stars in the case of spinning.

threshold should be lower than that of the preceding two examples. The same star sensor used in [27] is assumed and the parameters calculated for the stellar gyroscope are used in our case for the simplicity of simulation. The magnitude threshold and the integration time are set as $m_{\text{th}} = 4$ and 500 ms, respectively, considering the angular rate [27]. The main-FOV is $\phi_m = 45$ deg as in the previous examples, but the prefiltering FOV and the sub-FOV are set as $\phi_n = \phi_s = 30$ deg due to the lack of stars resulted from a lower detection threshold. The same attitude with the first example at the start of integration is assumed. The number of stars as a function of the integration time is shown in Fig. 14. In Fig. 14, the solid line shows the change of the number of stars in the main-FOV and the dotted line shows that in the prefiltering FOV. These changes are due to the in-and-out of stars during the integration time. The resulting estimated view position and other parameters are summarized in Table 3. Because the prefiltering gives much more candidates ($N_c = 1511$) than the first example when the same $\kappa(=0.2)$ is used, the result of coarse estimation is more accurate compared with that of the first example. However, the result of fine estimation shows a lower accuracy than that of the first example and it is on account that the variance of the number of stars in case of $m_{\text{th}} = 4$ is lower than that of $m_{\text{th}} = 6$.

VI. Conclusions

In this paper, an alternative approach to vector observations for attitude determination using star-density maps is presented. It uses a new measurement, i.e., the number of stars in the FOV, based on the distribution of the stars in the celestial coordinate system. Basically, attitude determination is performed by solving the least-squares problem using vector measurements. The proposed method includes two steps for the vector observations. In the coarse estimation stage, the vector measurement for the optical axis is performed through a sequence-matching method. The downhill simplex optimization method with the initial value estimated in the coarse stage is used in the fine estimation stage.

The proposed method retains the following features: With a little modification of detection threshold in the proposed algorithm, the number of stars as the selection of measurement makes it possible to apply this method to a rotational star tracker in which the accurate vector measurement of the star is impossible. It is not necessary to track the stars and to identify the stars with a pattern recognition algorithm. The creation of the star-density map according to the FOV will be executed on the ground before launching, so an onboard star catalog is not necessary. Although the assumptions we postulated for the measurement model may look absurd in the cases when there are some screened stars or the stars are too close together over the resolution of the star sensor to separate, the adoption of sub-FOVs reduces errors because they divide the main-FOV area and allow multiple vector observations with a single star sensor. The probability that there is an error of measurement in one of the sub-FOVs is lowered as the number of sub-FOVs increases. Moreover, because the proposed method is a single-frame attitude

Table 3 True attitude parameters and estimated parameters in the case of spinning

Parameter	True value	
Position of optical axis, $\boldsymbol{x}_m$	$[185.1834, -1.6179]^T$ deg	
Position of y-axis, $\boldsymbol{x}_y$	$[275.1894, -0.2130]^T$ deg	
Position of z-axis, $\boldsymbol{x}_z$	$[192.6864, 88.3681]^T$ deg	
Rotation angle, θ	179.7135 deg	
DCM, A	$\begin{bmatrix} -0.9955 & -0.0903 & -0.0282 \\ 0.0904 & -0.9959 & -0.0037 \\ -0.0278 & -0.0063 & 0.9996 \end{bmatrix}$	
FOV	$\phi_m = 45$ deg	$\phi_s = \phi_n = 30$ deg
Magnitude threshold, m_{th}	4	
	Coarse estimation	*Fine estimation*
Position of optical axis, $\hat{\boldsymbol{x}}_m$	$[185, -2]^T$ deg	$[185.4274, -1.5694]^T$ deg
Position of y-axis, $\hat{\boldsymbol{x}}_y$	$[274.9697, 0.8683]^T$ deg	$[275.4302, -0.1029]^T$ deg
Position of z-axis, $\hat{\boldsymbol{x}}_z$	$[161.5126, 87.8195]^T$ deg	$[189.1788, 88.4272]^T$ deg
Rotation angle, $\hat{\theta}$	180.7807 deg	179.8229 deg
DCM, $\hat{A}$	$\begin{bmatrix} -0.9956 & -0.0871 & -0.0349 \\ 0.0866 & -0.9961 & -0.0152 \\ -0.0361 & -0.0121 & 0.9993 \end{bmatrix}$	$\begin{bmatrix} -0.9951 & -0.0945 & -0.0274 \\ 0.0946 & -0.9955 & -0.0018 \\ -0.0271 & -0.0049 & 0.9996 \end{bmatrix}$
Convergence index, C	8.3018×10^{-4}	4.4178×10^{-5}

determination solution, which obtains all vector measurements at the same attitude, this method does not use the kinematic model of the rigid body and does not require any angular rate information. Therefore, the proposed method only needs a single star sensor for attitude determination without the help of redundant sensors such as a gyro.

Acknowledgment

This work was supported in part by Agency for Defense Development through a grant managed by Radiowave Detection Research Center, and by Korea Science and Engineering Foundation under contract R01-2003-000-10829-0 as well as a grant managed by MICROS ERC.

References

[1] Bar-Itzhack, I. Y., and Reiner, J., "Recursive Attitude Determination from Vector Observations: Direction Cosine Matrix Identification," *Journal of Guidance, Control, and Dynamics*, Vol. 7, No. 1, 1984, pp. 51–56.

[2] Bar-Itzhack, I. Y., and Oshman, Y., "Attitude Determination from Vector Observations: Quaternion Estimation," *IEEE Transactions on Aerospace and Electronic Systems*, Vol. 21, No. 1, 1985, pp. 128–135.

[3] Bar-Itzhack, I. Y., and Idan, M., "Recursive Attitude Determination from Vector Observations: Euler Angle Estimation," *Journal of Guidance, Control, and Dynamics*, Vol. 10, No. 2, 1987, pp. 152–157.

[4] Idan, M., "Estimation of Rodrigues Parameters from Vector Observations," *IEEE Transactions on Aerospace and Electronic Systems*, Vol. 32, No. 2, April 1996, pp. 578–586.

[5] Crassidis, J. L., and Markley, F. L., "Attitude Estimation Using Modified Rodrigues Parameters," *Proceedings of Flight Mechanics/Estimation Theory Symposium*, NASA Goddard Space Flight Center, Greenbelt, MD, May 1996, pp. 71–83.

[6] Shuster, M. D., and Oh, S. D., "Three-Axis Attitude Determination from Vector Observations," *Journal of Guidance, Control, and Dynamics*, Vol. 4, No. 1, Jan.–Feb. 1981, pp. 70–77.

[7] Wahba, G., "A Least Squares Estimate of Spacecraft Attitude," *SIAM Review*, Vol. 7, No. 3, 1965, p. 409.

[8] Wertz, J. R., *Spacecraft Attitude Determination and Control*, D. Reidel, Dordrecht, Holland, 1978, pp. 426–428.

[9] Lefferts, E. J., Markley, F. L., and Shuster, M. D., "Kalman Filtering for Spacecraft Attitude Estimation," *Journal of Guidance, Control, and Dynamics*, Vol. 5, No. 5, Sept.–Oct. 1982, pp. 417–429.

[10] Markley, F. L., "Attitude Determination Using Vector Observations and the Singular Value Decomposition," *Journal of the Astronautical Sciences*, Vol. 36, No. 3, July–Sept. 1988, pp. 245–258.

[11] Markley, F. L., "Attitude Determination Using Vector Observations: A Fast Optimal Matrix Algorithm," *Journal of the Astronautical Sciences*, Vol. 41, No. 2, April–June 1993, pp. 261–280.

[12] Bar-Itzhack, I. Y., "REQUEST: A Recursive QUEST Algorithm for Sequential Attitude Determination," *Journal of Guidance, Control, and Dynamics*, Vol. 19, No. 5, 1996, pp. 1034–1038.

[13] Markley, F. L., and Bar-Itzhack, I. Y., "Unconstrained Optimal Transformation Matrix," *IEEE Transactions on Aerospace and Electronic Systems*, Vol. 34, No. 1, Jan. 1998, pp. 338–343.

[14] Psiaki, M. L., "Attitude-Determination Filtering via Extended Quaternion Estimation," *Journal of Guidance, Control, and Dynamics*, Vol. 23, No. 2, 2000, pp. 206–214.

[15] Crassidis, J. L., "Unscented Filtering for Spacecraft Attitude Estimation," *Journal of Guidance, Control, and Dynamics*, Vol. 26, No. 4, July–Aug. 2003, pp. 536–542.

[16] Choukroun, D., Bar-Itzhack, I. Y., and Oshman, Y., "Optimal-REQUEST Algorithm for Attitude Determination," *Journal of Guidance, Control, and Dynamics*, Vol. 27, No. 3, May–June 2004, pp. 418–425.

[17] Creamer, G., "Spacecraft Attitude Determination Using Gyros and Quaternion Measurements," *Journal of the Astronautical Sciences*, Vol. 44, No. 3, 1996, pp. 357–371.

[18] Gebre-Egziabher, D., Hayward, R. C., and Powell, J. D., "Design of Multi-Sensor Attitude Determination Systems," *IEEE Transactions on Aerospace and Electronic Systems*, Vol. 40, No. 2, April 2004, pp. 627–649.

[19] Liebe, C. C., "Star Trackers for Attitude Determination," *IEEE Aerospace and Electronics Systems Magazine*, Vol. 10, No. 6, June 1995, pp. 10–16.

[20] Scholl, M. S., "Star-Field Identification for Autonomous Attitude Determination," *Journal of Guidance, Control, and Dynamics*, Vol. 18, No. 1, 1995, pp. 61–65.

[21] Liebe, C. C., "Pattern Recognition of Star Constellations for Spacecraft Applications," *IEEE Aerospace and Electronics Systems Magazine*, Vol. 8, No. 1, Jan. 1993, pp. 31–39.

[22] Cho, S., and Chun, J., "Satellite Attitude Acquisition Using Dual Star Sensors with a Bootstrap Filter," *Proceedings of IEEE Sensors 2002*, Vol. 2, June 2002, pp. 1723–1727.

[23] Shuster, M. D., "A Survey of Attitude Representations," *Journal of the Astronautical Sciences*, Vol. 41, No. 4, 1993, pp. 439–517.

[24] Wertz, J. R., *Spacecraft Attitude Determination and Control*, D. Reidel, Dordrecht, Holland, 1978, pp. 143–146.

[25] Ash, R. B., *Real Analysis and Probability*, Academic Press, New York, 1972, pp. 336–341.

[26] Press, W. H., Teukolsky, S. A., Vetterling, W. T., and Flannery, B. P., *Numerical Recipes in C: The Art of Scientific Computing*, Cambridge Univ., London, 1996, pp. 408–412.

[27] Liebe, C. C., Gromov, K., and Meller, D. M., "Toward a Stellar Gyroscope for Spacecraft Attitude Determination," *Journal of Guidance, Control, and Dynamics*, Vol. 27, No. 1, Jan.–Feb. 2004, pp. 91–99.

[28] Liebe, C. C., "Accuracy Performance of Star Trackers—A Tutorial," *IEEE Transactions on Aerospace and Electronic Systems*, Vol. 38, No. 2, 2002, pp. 587–599.